ELSEVIER

Journal of Fluids and Structures 25 (2009) 1243–1257

JOURNAL OF FLUIDS AND STRUCTURES

www.elsevier.com/locate/jfs

Aeroelastic analysis of helicopter rotor blade in hover using an efficient reduced-order aerodynamic model

H. Shahverdi[a,*], A.S. Nobari[b], M. Behbahani-Nejad[c], H. Haddadpour[d]

[a]*Department of Mechanical and Aerospace Engineering, Islamic Azad University, Science and Research Branch, Tehran 14515-775, Iran*
[b]*Aerospace Engineering Department & Center of Excellence in Computational Aerospace, Amir Kabir University of Technology, Tehran 15875-4413, Iran*
[c]*Mechanical Engineering Department, Shahid Chamran University of Ahvaz, Ahvaz 61355-148, Iran*
[d]*Aerospace Engineering Department, Sharif University of Technology, Tehran 11365-8639, Iran*

Received 12 July 2008; accepted 12 June 2009
Available online 31 August 2009

Abstract

This paper presents a coupled flap–lag–torsion aeroelastic stability analysis and response of a hingeless helicopter blade in the hovering flight condition. The boundary element method based on the wake eigenvalues is used for the prediction of unsteady airloads of the rotor blade. The aeroelastic equations of motion of the rotor blade are derived by Galerkin's method. To obtain the aeroelastic stability and response, the governing nonlinear equations of motion are linearized about the nonlinear steady equilibrium positions using small perturbation theory. The equilibrium deflections are calculated through the iterative Newton–Raphson method. Numerical results comprising steady equilibrium state deflections, aeroelastic eigenvalues and time history response about these states for a two-bladed rotor are presented, and some of them are compared with those obtained from a two-dimensional quasi-steady strip aerodynamic theory. Also, the effect of the number of aerodynamic eigenmodes is investigated. The results show that the three-dimensional aerodynamic formulation has considerable impact on the determination of both the equilibrium condition and lead-lag instability.

Keywords: Aeroelastic; Aerodynamic; Blade; Eigenvalue; Flutter

1. Introduction

Determination of the aeroelastic stability of a hingeless blade is a complex aeroelastic problem due to the interaction of unsteady aerodynamic, structure, and inertia forces and their nonlinear properties. Most of the recent studies on blade aeroelastic stability emphasize one of the disciplines and assume some simplification in the others (Hodges and Dowell, 1974; Cho and Lee, 1994); but advanced aerodynamic and structural models are both required to perform reliable analyses.

In most of the earlier studies, the simple two-dimensional quasi-steady aerodynamic models have been incorporated in the aeroelastic models (Friedmann and Tong, 1972; Hodges and Ormiston, 1976). Most of these models are based on

*Corresponding author.
E-mail address: shahverdi_ho@srbiau.ac.ir (H. Shahverdi).

0889-9746/$ - see front matter © 2009 Elsevier Ltd. All rights reserved.
doi:10.1016/j.jfluidstructs.2009.06.007

Nomenclature

A	aerodynamic influence coefficient matrix
a	two-dimensional lift curve slope
C_{d_0}	profile drag coefficient
B	coefficient matrix relating the strength of the wake elements in different time step
$C(q)$	gyroscopic matrix
$c(t)$	normal mode coordinates vector
c	blade chord length
E	influence of the flux density coefficient matrix
F_A	aerodynamic load vector
F_{ec}	elastic and centrifugal force vector
$K(q)$	stiffness matrix
K_A	radius of gyration of blade cross-section
K_m	mass radius of gyration of blade cross-section
K_{m_1} , K_{m_2}	principal mass radii of gyration
M	mass matrix
m	reference mass per unit length of blade
q	generalized coordinate vector
q_0	generalized coordinate vector about equilibrium condition
$\hat{q}$	small perturbation of generalized coordinate vector
R	blade radius
Y	right eigenvector matrix
Z	eigenvalue matrix
γ	lock number, $\gamma = 3\rho acR/m$
ρ	air density
Φ	unsteady perturbation potential about the free stream
Φ_0	strength vector about equilibrium condition
$\hat{\Phi}$	small perturbation about steady equilibrium position Φ_0
ψ	dimensionless time, $\psi = \Omega t$
Ω	angular velocity
$\omega_v,\omega_w,\omega_\phi$	nondimensional rotating lead-lag, flap, and torsion frequencies, respectively

Greenberg's theory which is used for fixed-wing type of unsteady theory (Greenberg, 1947), enhanced with a simple momentum wake model for rotor blade applications. Since the dynamic effects of unsteady wake are very important for aeroelastic analysis of the rotor blade, those earlier aerodynamic models which did not consider the effect of unsteady wake and its geometry are not reliable. To consider the effect of the spiral returning wake beneath a hovering rotor, Loewy (1957) represented a new two-dimensional blade aerodynamic model based on the modification of the analytical Theodorsen aerodynamic theory for hovering flight conditions. Moreover, with improvements in high-speed computer technology, more advanced numerical rotor aerodynamic models have been developed and used in aeroelastic analysis. These models account for wake contraction, wake distortion, blade–vortex interaction, rotor–body interaction and three-dimensional effects along the blade and tip-relief effects. Kwon et al. (1991) studied the aeroelastic behavior of hingeless rotor blades in hover using the boundary element method (BEM) based on the panel method for three-dimensional aerodynamic computations. In the same study, Yoo et al. (1992) applied the vortex lattice method to find aeroelastic response and conduct a stability analysis. In these studies, the wake geometry of the rotor can be prescribed from visualization studies of similar rotors at the same flight condition, or the known generalized equations (Landgrebe, 1972; Kocurek and Tangler, 1977). Also, it can be obtained as part of the solution from a free wake calculation (Katz and Plotkin, 2002). Also, De Andrade and Peters (1993) performed aeroelastic analysis based on the generalized dynamic inflow model, including a three-dimensional shed wake inflow. In addition, the aeroelastic response and stability of multibladed hingeless rotors in hover have been investigated using the three-dimensional unsteady vortex lattice method (Cho and Lee, 1995). These studies have shown some improvements in prediction of the lead-lag damping values over the full range of collective pitch angles, compared with those obtained from two-dimensional quasi-steady aerodynamic models.

Despite the fact that there are different aerodynamic solvers based on the Euler and Navier–Stokes formulations to solve aeroelastic problems (Smith, 1996; Pomin and Wagner, 2002), BEM has been known as a powerful numerical technique in engineering analysis. In CFD analyses and especially in heat transfer problems, BEM plays an important and efficient role. At the beginning, this method was used only in linear problems, but it developed quickly to also analyze nonlinear problems. One of its main advantages is the reduction of the problem dimensionality by one, since it will be required to discretize only the boundary of the computational domain. Based on the above statements, BEM has recently been used in many studies for unsteady flow computations and aeroelastic investigations (Chen, 2001; Eller and Carlsson, 2003). The combination of the BEM and reduced-order modeling (ROM) gives faster solutions for unsteady flow computations about real and complex geometries and it can be employed in aeroelastic modeling (Hall, 1994; Tang et al., 1999; Tang and Dowell, 2001; Esfahanian and Behbahani-Nejad, 2002). The ROM technique is similar to modal analysis, which is commonly used in the field of structural dynamics. In this regard, unsteady flow eigenmodes are used to construct reduced-order models. Using this approach, one may construct a reduced-order model using a set of a few dominant modes to accurately and rapidly predict the unsteady aerodynamic response over a wide range of the reduced

frequencies. Besides, the eigenmode information provides important insights into the physics of unsteady flows. Other methods such as proper orthogonal decomposition (POD) and balanced modes have been used for investigation of unsteady flows (Dowell et al., 1999a, 1999b, 2006).

Proper orthogonal decomposition (POD) is an attractive alternative to the use of eigenmodes to provide a reduced-order aeroelastic model that reduces the computational model size and cost by several orders of magnitude. This method has been used for a wide range of dynamic system characterization and data compression applications (Romanowski, 1996), and is more efficient for extracting eigenmodes for very high dimension systems (greater than 10^4). Kim (1998) has used the POD frequency domain method for a vortex lattice fluid model. Thomas et al. (1999b) have used it for an Euler fluid model including shock wave at transonic conditions. Feng and Soulaimani (2007) used POD method which was based on a three-field coupled full-order model to construct a reduced-order model of a three-dimensional nonlinear aeroelasticity system with moving fluid boundaries in transonic flow.

Behbahani-Nejad et al. (2005) and Shahverdi et al. (2007) presented an accelerated and efficient modified reduced-order modeling (MROM) approach for unsteady aerodynamic calculations based on the boundary element method. They showed that this method is more efficient than the conventional method. In this new approach the governing eigenvalue problem of unsteady flows is defined based on the unknown wake singularities. Thus, by constructing this reduced-order model, the body's quasi-static eigenmodes are removed from the eigensystem, and it is possible to obtain satisfactory results without using the static correction technique when enough eigenmodes are used. Also, the coefficient matrix in MROM has smaller dimension with respect to the conventional reduced-order model (CROM) [see Hall (1994)]. Therefore, one can use the static correction technique more effectively along with this approach to obtain satisfactory results with a lower number of eigenmodes. By incorporating this aerodynamic model into the aeroelastic equations, a faster and more powerful solver can be built for aeroelastic stability analysis.

The main objective of the present work is to develop an efficient and powerful framework for aeroelastic response calculations. It uses a MROM aerodynamic solver, which is based on BEM, for unsteady flow computations around a helicopter rotor blade and the modal technique to simulate structural dynamics behavior. A geometrically nonlinear beam model has been considered for coupled flap–lag–torsion equations of motion of a hingeless rotor blade. It allows for moderately large deflections based on the ordering scheme that limits the magnitudes of displacements and rotations. The nonlinear equations of motion are formulated with the aid of Galerkin's method, based on the coupled rotating blade mode shapes. Moreover, the paper describes how the aeroelastic model is formulated by coupling the MROM aerodynamic equations to the structural equations of a rotor blade. Hence, using Galerkin's method, the system of nonlinear integro-partial-differential equations is reduced to ordinary differential equations. To solve these equations, the nonlinear steady equilibrium deflections due to steady aerodynamic loads and centrifugal forces are first determined through the iterative Newton–Raphson method. Then, the aeroelastic behavior of the rotor blade is investigated by linearizing the complete equations about the equilibrium operating condition, using small perturbation theory.

For a given hingeless blade configuration, aeroelastic stability is addressed by means of eigenanalysis and time history results. Also, a comparison has been made using different reduced-order mode numbers. Presented numerical results consist of steady equilibrium deflections, aeroelastic eigenvalues and time domain response about these deflections for a two-bladed rotor. Some of the results are compared with those obtained by applying a two-dimensional quasi-steady Greenberg's aerodynamic theory.

2. Unsteady aerodynamic model

For the case of an incompressible, inviscid, irrotational flow, the Navier–Stokes equations can be reduced to the classical Laplace equation (potential flow theory). Using BEM, the body surface and the wake are represented via quadrilateral constant elements. From Green's second identity, it can be shown that the solution to Laplace's equation in the flow field can be obtained from the following system of equations (Esfahanian and Behbahani-Nejad, 2002):

$$A\Phi^{n+1} + B\Phi^{n} = w^{n+1}, \tag{1}$$

where A and B are the influence coefficient matrices of the system. The vector Φ is defined as

$$\Phi = \{\bar{\Phi}_1, \bar{\Phi}_2, \ldots, \bar{\Phi}_{NB}, \Delta\bar{\Phi}_1, \Delta\bar{\Phi}_2, \ldots, \Delta\bar{\Phi}_{NW}\}, \tag{2}$$

where $\bar{\Phi}_i$ and $\Delta\bar{\Phi}_i$ are the ith unknown potential of body and wake element, respectively.

Given a prescribed time history of the body motion, Eq. (1) is simply marched in time from one time level (n) to the next ($n+1$) and then the time history of the potential strengths of each element will be found. When the velocity

potential is determined, the resulting pressure coefficient and related aerodynamic forces can be computed from modified Bernoulli's equation (Katz and Plotkin, 2002).

Define Φ_b as the vector of the unknown potential laying on the body surface along with the potential of the attached wake element to the trailing edge (Kutta panels or elements) and Φ_w as the vector of the wake unknown potential differences. Using these definitions, one can write

$$\Phi = \begin{Bmatrix} \Phi_b \\ \Phi_w \end{Bmatrix}. \tag{3}$$

Now, Eq. (1) can be written as (Shahverdi et al., 2007)

$$\begin{bmatrix} A_{11} & A_{12} \\ A_{21} & A_{22} \end{bmatrix} \begin{Bmatrix} \Phi_b \\ \Phi_w \end{Bmatrix}^{n+1} + \begin{bmatrix} B_{11} & B_{12} \\ B_{21} & B_{22} \end{bmatrix} \begin{Bmatrix} \Phi_b \\ \Phi_w \end{Bmatrix}^{n} = \begin{Bmatrix} w_b \\ 0 \end{Bmatrix}^{n+1}, \tag{4}$$

where w_b denotes the vector of potential flux values (or downwash) on the body. Expressing Eq. (4) into two equations yields

$$A_{11}\Phi_b^{n+1} + A_{12}\Phi_w^{n+1} + B_{11}\Phi_b^n + B_{12}\Phi_w^n = w_b^{n+1}, \tag{5}$$

$$A_{21}\Phi_b^{n+1} + A_{22}\Phi_w^{n+1} + B_{21}\Phi_b^n + B_{22}\Phi_w^n = 0. \tag{6}$$

Based on the wake potential difference interaction at n and $n+1$, it can be shown that the elements B_{11}, B_{12} and A_{21} are zero (Shahverdi, 2006), and therefore, Eq. (5) gives

$$\Phi_b^{n+1} = A_{11}^{-1} w_b^{n+1} - A_{11}^{-1} A_{12} \Phi_w^{n+1}. \tag{7}$$

Substitution of Eq. (7) into Eq. (6) gives

$$A_{\text{new}}\Phi_w^{n+1} + B_{\text{new}}\Phi_w^n = w_{\text{new}}^n, \tag{8}$$

where

$$\begin{aligned} A_{\text{new}} &= A_{22}, \\ B_{\text{new}} &= B_{22} - B_{21}A_{11}^{-1}A_{12}, \\ w_{\text{new}}^n &= -B_{21}A_{11}^{-1}w_b^n. \end{aligned} \tag{9}$$

Also, w_b is defined as

$$w_b^n = -E_1 - E_2 q^n, \tag{10}$$

where E_1 is a vector representing the perturbation potential of the elements due to free stream velocity, and E_2 is a matrix describing the linear relationship between the motion of the airfoil and the perturbation velocity potential at the center of each element laid on the body.

Since Eq. (8) is expressed only in terms of the wake potential differences, the corresponding eigensystem has no zero eigenvalue, and one may construct accurate reduced-order models without using a static correction technique (Shahverdi, 2006).

3. Structural model

The blade structural model used in the present analysis is based on Dowell and Hodges's beam model (Hodges and Dowell, 1974). Therefore, the blade is modeled as a geometrically nonlinear Euler–Bernoulli beam based on moderately large deflections and small strains. Also, transverse shear deformations and torsional warping effects are neglected in this formulation. Thus, the coupled flap–lag–torsion integro-partial-differential equations of motion are derived analytically from Hamilton's principle. Moreover, the blade is assumed to be attached to a fixed axis in space and rotating at constant angular velocity about it. Fig. 1 shows the bending and torsional deflections of the blade. There, V, W, and ϕ denote lead-lag, flap, and torsional deflection of the beam reference line, respectively.

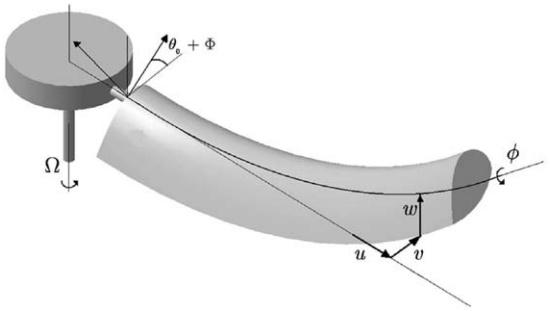

Fig. 1. Schematic of rotor blade indicating orientation of elastic deformations.

4. Aeroelastic model

After introducing the present reduced-order modeling approach, we will now describe briefly how the MROM model can be used to construct an aeroelastic model for flutter instability calculations. Applying the standard Galerkin method to the coupled equations of motions can give the nonlinear ordinary differential equations in the following matrix form (Shahverdi, 2006):

$$M\ddot{q} + C(q)\dot{q} + K(q) = F_{ec}(q) + F_A(q, \dot{q}, \Phi, \dot{\Phi}), \tag{11}$$

where M, C, and K are the mass, gyroscopic damping, and stiffness matrices, respectively. Also, q is the generalized deflection vector, and Φ is the aerodynamic potential vector. In addition, the term F_{ec} denotes the summation of elastic and centrifugal force vectors, and the vector F_A represents the generalized aerodynamic forces due to the sectional aerodynamic forces and pitching moment. These aerodynamic forces are complex nonlinear functions of the relative air-stream velocities and blade deformations. In the present work an explicit algebraic form for these functions is derived, which reduces computational effort and complexity [for more details see Hodges and Dowell (1974)].

To solve Eq. (11), first the nonlinear steady-state quantities such as q_0 and Φ_0 should be determined using the steady forces. Then, by dropping all time-dependent terms, the steady equilibrium equations can be obtained. These quantities can be determined through an iterative Newton–Raphson procedure. Consequently, for small perturbations about the steady equilibrium solution, the time-dependent quantities are expressed in terms of the steady-state quantities and their small unsteady perturbation elements as

$$q = q_0 + \hat{q}, \quad \Phi = \Phi_0 + \hat{\Phi}. \tag{12}$$

Thus, linearization of the perturbation equations about the nonlinear steady equilibrium solution, q_0, Φ_0, leads to the following equations (Shahverdi, 2006):

$$M\ddot{q} + C(q_0)\dot{\hat{q}} + K(q_0) = F_{A_1}(q_0, \Phi_0)\hat{q} + F_{A_2}(q_0, \Phi_0)\hat{\Phi} + F_{A_3}\dot{\hat{\Phi}}. \tag{13}$$

In a similar manner, the basic governing equations of the aerodynamic model, Eq. (1), can be reduced to the following form:

$$A\hat{\Phi}^{n+1} + B\hat{\Phi}^{n} + E\hat{q}^{n+1} = 0, \tag{14}$$

where E is a matrix describing the linear relationship between the blade motion and perturbation velocity potential at each collocation point laid on the blade surface. Since the aerodynamic equation has been defined in a discrete time domain, the combination of the aerodynamic and structural equations (Eq. (13)), can also be written in this domain. Writing the equation at time interval $(n+1/2)\,\Delta t$ and employing the central difference approximation lead to

$$(D_2 + F_1)\hat{q}^{n+1} + (D_1 + F_{A_1})\hat{q}^{n} + F_{A_2}\hat{\Phi}^{n+1} + F_{A_3}\hat{\Phi}^{n} = 0, \tag{15}$$

where D_2 and D_1 are constant coefficient matrices defined in Shahverdi (2006).

Combining Eqs. (14) and (15) in matrix form leads to

$$\begin{bmatrix} A & E \\ F_{A_2} & (D_2 + F_{A_1}) \end{bmatrix} \begin{Bmatrix} \hat{\Phi} \\ \hat{q} \end{Bmatrix}^{n+1} + \begin{bmatrix} B & 0 \\ F_{A_3} & (D_1 + F_{A_1}) \end{bmatrix} \begin{Bmatrix} \hat{\Phi} \\ \hat{q} \end{Bmatrix}^{n} = 0. \tag{16}$$

For aeroelastic stability analysis, one must compute the eigenvalues of Eq. (16) in different flight conditions and blade configurations. Also, for aeroelastic response computations in the time domain, we can define the time derivative quantities as follows:

$$\dot{q}(\psi+\Delta\psi)=\frac{q(\psi+\Delta\psi)-q(\psi)}{\Delta\psi}=y_1(\psi+\Delta\psi) \tag{17}$$

and

$$\dot{\hat{\Phi}}(\psi+\Delta\psi)=\frac{\hat{\Phi}(\psi+\Delta\psi)-\hat{\Phi}(\psi)}{\Delta\psi}=y_2(\psi+\Delta\psi). \tag{18}$$

Thus, putting Eqs. (17) and (18) into Eq. (13) gives

$$M\frac{\boldsymbol{y}_1(\psi+\Delta\psi)-\boldsymbol{y}_1(\psi)}{\Delta\psi}+C\boldsymbol{y}_1(\psi+\Delta\psi)+Kq(\psi+\Delta\psi)-F_{A_1}\hat{q}+F_{A_2}\hat{\Phi}+F_{A_3}\boldsymbol{y}_2(\psi+\Delta\psi)=0, \tag{19}$$

where $\psi=\Omega t$ is the dimensionless time.

Using eigenmodes of Eq. (8) along with orthogonality properties, this equation becomes (Shahverdi, 2006):

$$c(\psi+\Delta\psi)+Y^TA_{\text{new}}G(E_1+E_2q(\psi+\Delta\psi))+Zc(\psi)+Y^TG_1(E_1+E_2q(\psi))=0, \tag{20}$$

where c is the vector of normal mode coordinates, Y is a matrix with rows that are the left eigenvectors, and Z is a diagonal matrix containing the eigenvalues of the system. Also, G and G_1 are defined as

$$G=(A_{\text{new}}+B_{\text{new}})^{-1}B_{21}A_{11}^{-1},\quad G_1=B_{\text{new}}G-B_{21}A_{11}^{-1}. \tag{21}$$

Eq. (20) represents the complete aerodynamic model, along with the static correction technique [for details, see Shahverdi (2006)]. The governing system of equations, Eq. (17) to Eq. (20), can be solved numerically in the time domain for the proper initial conditions.

5. Solution procedure

In computing stability results, some simplifications are assumed in this study. For example, mass and stiffness properties are considered to be constant. Also, aerodynamic, elastic and mass centers are assumed to be coincident.

To obtain steady equilibrium conditions, first the aerodynamic loads must be determined. Hence, the blade is assumed to be undeformed initially, and the free–wake model is employed to yield the wake geometry. After computing the influence coefficients in Eq. (1), the potential strength distribution on the blade surface is determined. Then, the pressure distribution and the resulting forces and moments are obtained. Applying the Newton–Raphson iteration procedure to the steady equations of motion yields the steady blade deflections. Next, using the obtained deflections the blade geometry is updated. Since the aerodynamic influence coefficients depend on the geometry of the blade, the new set of the influence coefficients in A and the right-hand side of Eq. (1) are calculated from the deformed blade geometry. Thus, a new set of aerodynamic equations is obtained. However, the coefficient matrix B in Eq. (1) does not change because it depends on Kelvin's theorem, which relates the strength of wake potentials from one time level (n) to the next ($n+1$). Then the new aerodynamic loads are found for the current state of blade deformation. This iterative process is repeated until satisfactory convergence is obtained under equilibrium conditions. It should be noted that the geometry of the near wake attached to the blade is assumed to follow the deflections of the blade trailing edge. On the other hand, the effect of blade deflections on the far wake geometry is assumed to be negligible because the magnitude of the deflections is small compared to the distance between the far wake and the blade (Kwon et al., 1991).

After this stage, the linearized equations of motions (Eq. (13)), are obtained using small perturbation theory. For the time integration of Eqs. (17)–(20), the initial perturbation values, $\hat{q}$ and $\hat{\phi}$, are taken to be 10% of the steady equilibrium conditions.

In the case of aeroelastic computations, the blade surface geometry and the corner points of each element will change from one time step to the next. Thus, the aerodynamic influence coefficients must be recomputed for each time step. Since the blade deflections are very small under the assumed small perturbation deflections, these coefficients are computed only once in each equilibrium condition. Therefore, the time history response of the blade can be obtained easily.

6. Results and discussion

In the present study, a rotor blade with an untwisted rectangular platform is used to investigate the effects of the three-dimensional tip loss effect and unsteady wake dynamics on the equilibrium deflections, aeroelastic eigenvalues, and blade dynamic response. The equilibrium deflections and lead-lag damping are also compared with those obtained from two-dimensional aerodynamic strip theory (Hodges and Ormiston, 1976).

Initially, to verify the aerodynamic load computation capability of the present BEM code, unsteady pressure coefficients at two sections in the spanwise direction are presented for the untwisted rectangular blade of a two-bladed rotor (with NACA0012 airfoil section, pitch angle 8° and aspect ratio 6) in hovering flight conditions. These are compared in Figs. 2 and 3 with the experimental results of Caradonna and Tung (1981). The results show good agreement between experiment and present study. Also, the wake geometry is obtained as a part of solution from free-wake calculations shown in Fig. 4. In this study, the body surface of each blade is discretized by 28 elements in the chordwise and 10 elements in the spanwise directions. Moreover, the blade root cutout is considered to be 10% of the blade radius.

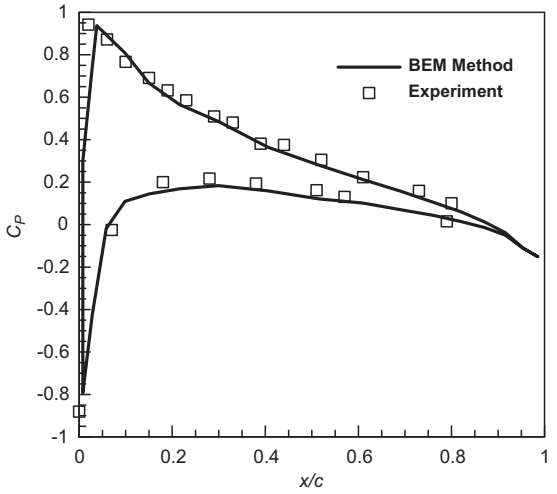

Fig. 2. Pressure distribution at section $r/R = 0.68$; experimental data from Caradonna and Tung (1981).

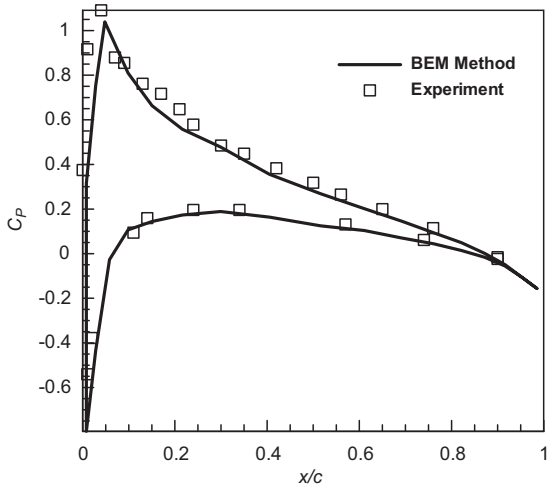

Fig. 3. Pressure distribution at section $r/R = 0.80$; experimental data from Caradonna and Tung (1981).

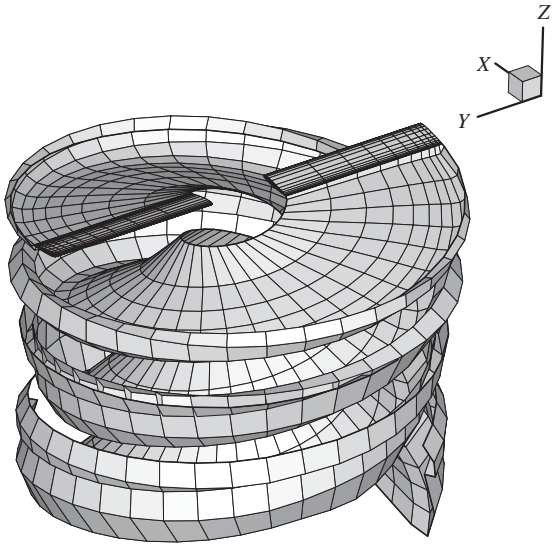

Fig. 4. Obtained free wake model of a two-bladed rotor.

Table 1
Two-bladed rotor parameters.

ω_v	0.7, 1.5
ω_w	1.15
ω_ϕ	2.5, 5.0, 8.0
$(K_A/K_m)^2$	1.5
K_m/R	0.025
K_{m_1}/K_{m_2}	0.0
$\gamma = (3\rho_\infty acR/m)$	5
c/R	$\pi/40$
C_{d_0}/a	$0.01/2\pi$

The configuration and operating condition parameters that are needed in the present aeroelastic study are given in Table 1. In order to compute aerodynamic loads, the surface of the blade is discretized similarly to the above presented model. Also, the wake is considered up to two blade revolutions (Katz and Maskew, 1988). The three-dimensional wake geometry is derived using the free wake methodology (Katz and Plotkin, 2002).

First, the equilibrium solution for the two-bladed soft in-plane rotor ($\omega_v = 0.7$, $\omega_w = 1.15$, and $\omega_\phi = 5$) is obtained. Then, the tip flap and lead-lag deflections are computed and normalized with respect to the blade radius, while the tip torsional deflection is determined in degrees.

Figs. 5–7 show the tip flap, lead-lag, and torsion deformations, respectively. As indicated in these figures, the obtained steady-state deflections using the three-dimensional aerodynamic model (BEM) are lower than those obtained using two-dimensional theory, because of the three-dimensional tip loss and unsteady wake effect. Also, it is observed that there is a good agreement between the predicted lead-lag and flap deflections of the two aerodynamic models at low collective pitch angles. This agreement is due to the use of the same profile drag coefficient in both aerodynamic models. However, the difference between the results at high collective pitch angles appears since the two-dimensional aerodynamic model overestimates induced drag (Cho and Lee, 1995). Also, it is shown that the torsional deflections predicted by the present method are about two-thirds of those given by the two-dimensional theory. This is due to the three-dimensional tip-relief effect which produces a high nose-up pitching moment and thus reduces the magnitude of the negative pitch deflections (Kwon et al., 1991).

Next, the predicted lead-lag dampings of a two-bladed stiff in-plane rotor ($\omega_v = 1.5$, $\omega_w = 1.15$, and $\omega_\phi = 5$) are shown in Fig. 8 at various collective pitch angles, and the results are compared with those obtained using two-dimensional aerodynamic theory. These results are determined via the eigenvalue analysis (IMSL Lib., 1980). Since the

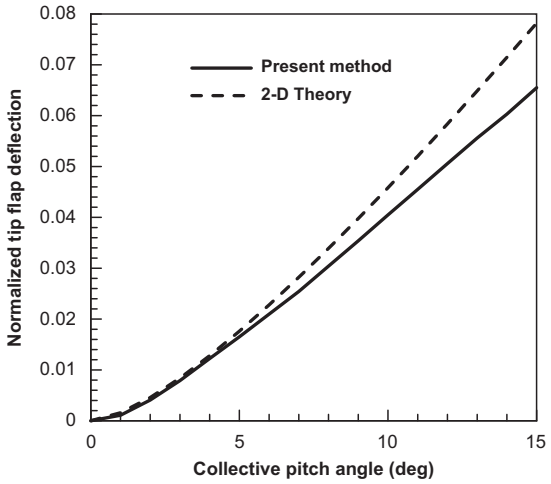

Fig. 5. Tip flap deflection at equilibrium position.

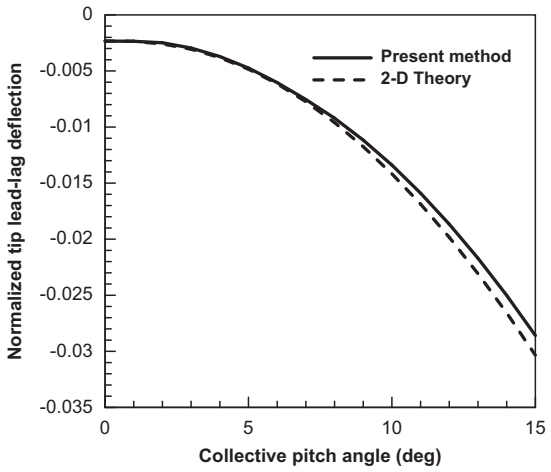

Fig. 6. Tip lead–lag deflection at equilibrium position.

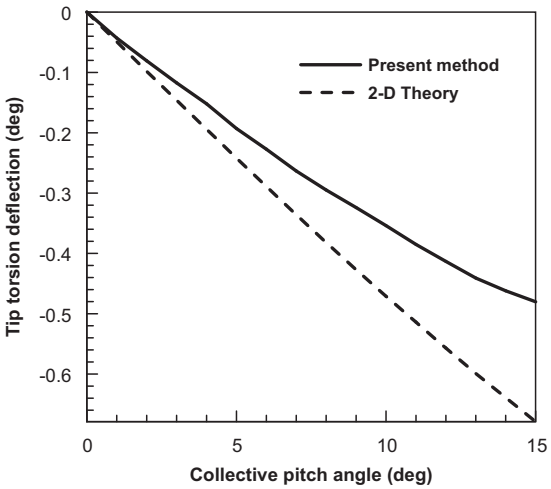

Fig. 7. Tip torsion deflection at equilibrium position.

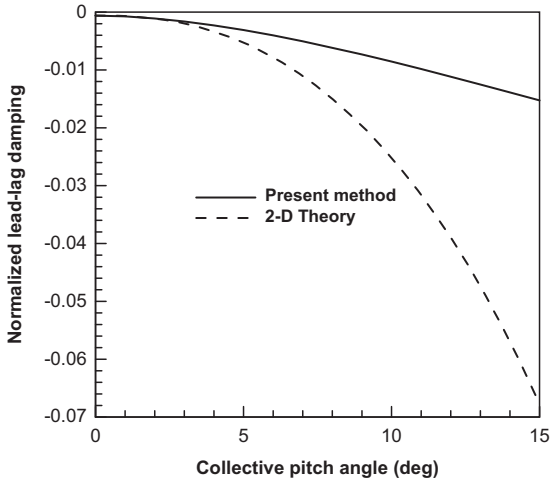

Fig. 8. Normalized lead–lag damping of a stiff in-plane rotor.

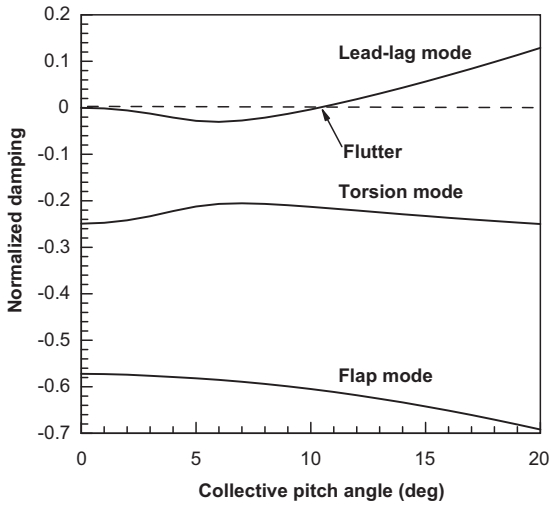

Fig. 9. Normalized damping of aeroelastic system of a two-bladed rotor.

same structural model without any structural damping is used in both models, the difference between results can be attributed to three-dimensional tip loss and unsteady wake dynamics occurring especially at high collective angles. At very low collective pitch angles, the aerodynamic force is mostly affected by the viscous profile drag; therefore, the same damping is predicted by both aerodynamic models.

Also, Figs. 9 and 10 show the real and imaginary parts of the aeroelastic eigenvalues of the same two-bladed rotor with given rotating frequencies as $\omega_v = 1.2$, $\omega_w = 1.15$, and $\omega_\phi = 2.5$ for various collective pitch angles. These results reveal that flutter occurs at a collective pitch angle of 11°. This phenomenon can also be observed from time marching solution. Hence, the time histories of lead-lag, flap and torsion perturbed motions of this rotor are computed at two different collective pitch angles. These results are obtained by using both the complete and MROM aeroelastic models. In addition, the effect of the number of aerodynamic eigenmodes on the obtained results is investigated. Here, the dimensionless time step is assumed to be 0.25°.

The time histories of the blade response at a collective pitch angle of 11° for three different perturbed motions are shown in Figs. 11–13. From these results, it is observed that the blade is neutrally stable. Also, these perturbed motions are calculated at a collective pitch angle of 13° using the complete aeroelastic model (direct method) and the results are shown in Figs. 14–16. The results show that the amplitude of each one of the perturbed motions increases rapidly with

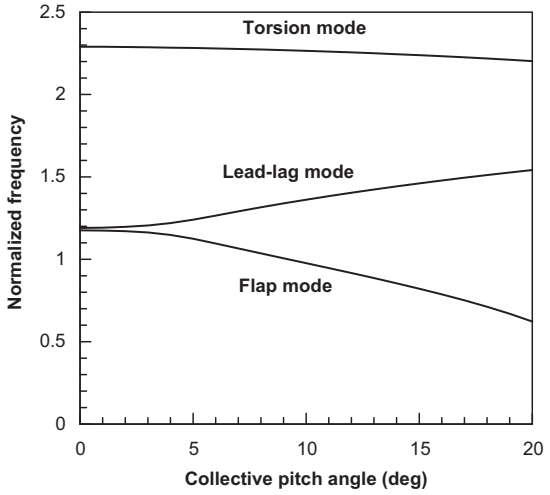

Fig. 10. Normalized frequency of aeroelastic system of a two-bladed rotor.

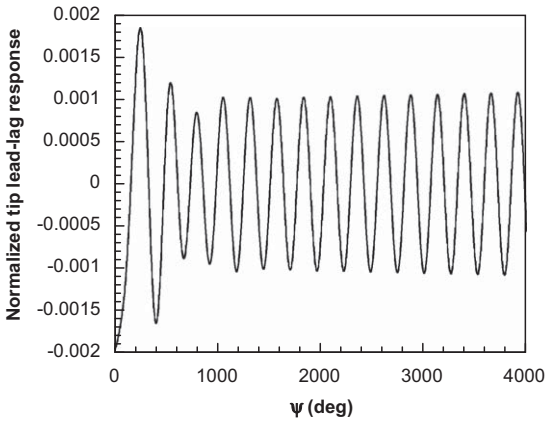

Fig. 11. Time history of lead–lag perturbation at 11° collective pitch angle.

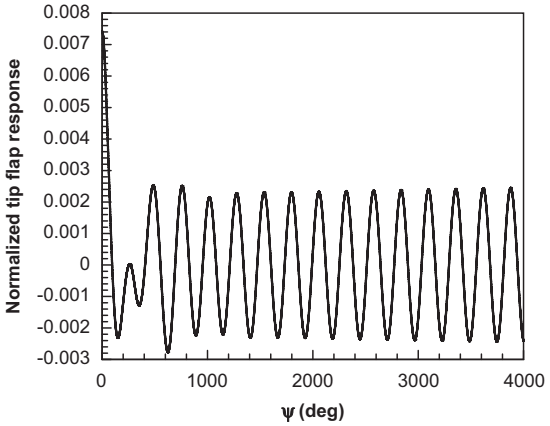

Fig. 12. Time history of flap perturbation at 11° collective pitch angle.

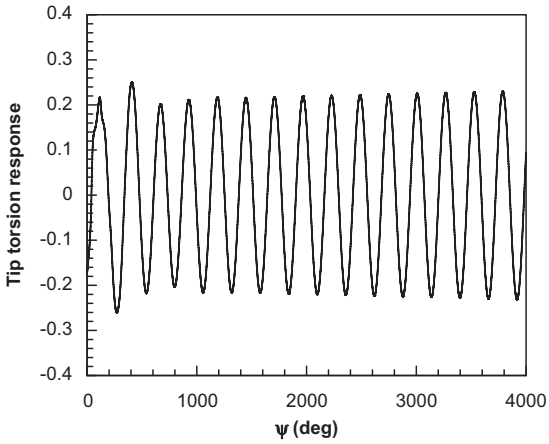

Fig. 13. Time history of torsion perturbation at 11° collective pitch angle.

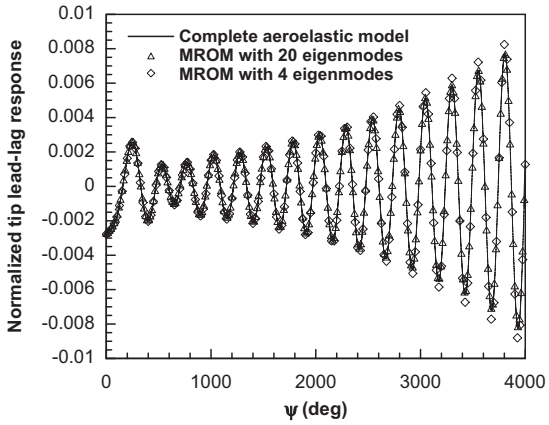

Fig. 14. Time history of lead–lag perturbation at 13° collective pitch angle.

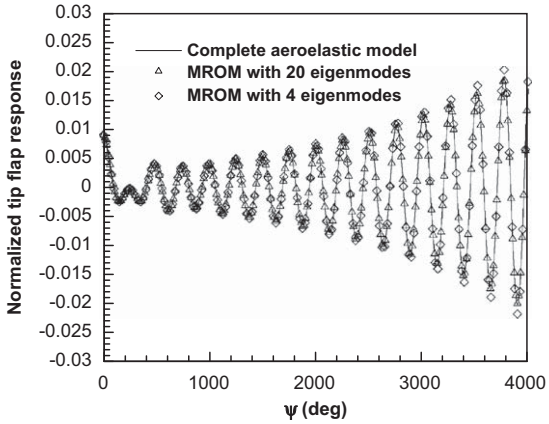

Fig. 15. Time history of flap perturbation at 13° collective pitch angle.

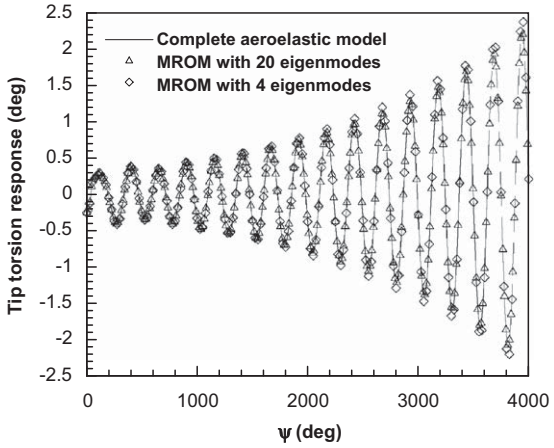

Fig. 16. Time history of torsion perturbation at 13° collective pitch angle.

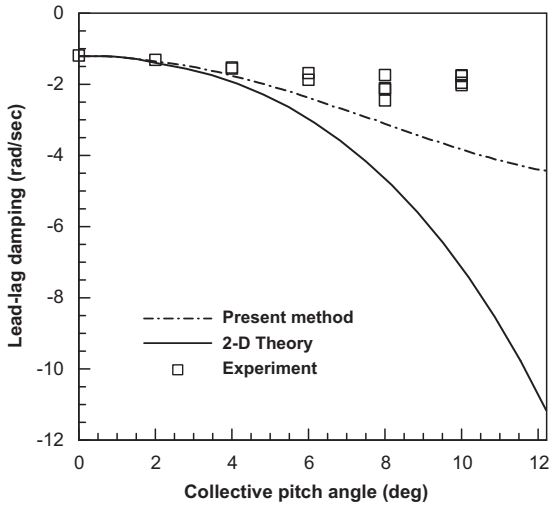

Fig. 17. Lead-lag damping of a stiff in-plane rotor; experimental data from Sharpe (1986).

time, which means that the aeroelastic response is unstable. The effect of the number of wake eigenmodes, which are used in the MROM aeroelastic model, is investigated here by considering 4 and 20 eigenmodes in the computations. As shown in Figs. 14–16, MROM with 20 eigenmodes gives satisfactory results when compared with the complete aeroelastic model.

For further verification of the results of the current work, a correlation study with experimental results is also performed. In this regard the values of configuration and operating condition parameters were taken from the experimental model that identified by Sharpe (1986) (blade set 2). The variations of the lead-lag damping of a stiff in-plane blade over the identified range of the collective pitch angle are shown in Fig. 17. The results demonstrate an improved ability of the present method to accurately determine the lead-lag damping with respect to the method associated with 2-D aerodynamic model. Above 4° the difference between the results of the present method and experiment increases as the value of the pitch angle increases. According to Sharpe (1986) and Kwon et al. (1991) this difference is related to the nonlinearity of the aerodynamic coefficients at the high collective pitch angles. However, the results associated with the present method show good agreement with the experimental results.

Finally, to show the efficiency of MROM using BEM in unsteady flow analysis over complex configuration, the last test case presented above is considered here. As a metric for the efficiency analysis, CPU times for the direct method and MROM with static correction technique along with 20 and 40 eigenmodes are compared (Table 2). The results are based on numerical computations using a P4-3200 MHz with 2-GB RAM. The results reveal that the present method can analyze the same problem significantly more efficiently than the direct method. The efficiency of the present method

Table 2
CPU time comparison between direct and present method.

Solution method	Number of eigenmodes	Time
Direct	–	125′, 31″
MROM	20	9′, 30″
MROM	4	2′, 16″

is due to the fact that the resulting MROM system of equations has a smaller dimension than the direct method. The maximum size of the coefficient matrix in the MROM aeroelastic model is equal to the number of structural degrees of freedom and aerodynamic eigenmodes, whereas in the complete aeroelastic model this size is equal to the number of structural degrees of freedom and number of aerodynamic elements that lay on the body surface and its wake. Therefore, MROM will be more efficient when the ratio of the number of body elements to the number of wake elements is increased, since it is based only on the wake elements. However, the application of the MROM without the static correction technique is more efficient than with static correction because there is no need to compute the quasi-steady solution in each time step when enough eigenmodes are used (Shahverdi, 2006).

7. Conclusion

Aeroelastic analysis of a simple helicopter hingeless blade has been performed to exemplify the usage of the three-dimensional boundary element method that accounts for the tip loss effect and unsteady wake inflow dynamics. The aeroelastic equations of the rotor blade were derived through Galerkin's method by considering large deflections and small strains. To eliminate the nonlinearity of the system of equations, small perturbation theory was used to linearize the equations about equilibrium. To increase the computational efficiency of the aeroelastic solver, the MROM methodology can be incorporated into the aeroelastic equations with a few eigenmodes. Thus, as a novel feature of the present work, an efficient reduced-order aerodynamic approach has been adopted for aeroelastic analysis of a helicopter rotor blade. In the present method, the numerical eigensystem is constructed only by the wake potentials, which results in a smaller dimension of the corresponding eigensystem. It can be concluded that the present method is computationally more efficient than the complete aeroelastic model. The steady equilibrium deflections and lead-lag damping of a two-bladed rotor are compared with those obtained from the two-dimensional aerodynamic theory. The results show that the three-dimensional aerodynamic effects greatly affect the equilibrium and blade aeroelastic stability, especially in high collective pitch angles.

The aeroelastic stability analysis based on the 3-D unsteady aerodynamic model yields more accurate lead-lag damping values of the two-bladed rotor compared to those obtained from a 2-D aerodynamic model.

The results show that the MROM aeroelastic model with a sufficient number of eigenmodes can produce satisfactory results and save considerable computational time. Moreover, it can be concluded that this efficiency will be more evident when the present technique is employed for unsteady flow computations around a complex configuration, including rotor–body interaction cases where a large number of aeroelastic calculations need to be performed.

Acknowledgement

The authors would like to thank the support and encouragement provided by Islamic Azad University Science and Research branch, Amirkabir University of Technology, Sharif University of Technology, and Shahid Chamran University of Ahvaz.

References

Behbahani-Nejad, M., Haddadpour, H., Esfahanian, V., 2005. Reduced-order modeling of unsteady flows without static correction requirement. Journal of Aircraft 42, 882–886.

Caradonna, F.X., Tung, C., 1981. Experimental and analytical studies of a model helicopter rotor in hover. NASA TM-81232.

Chen, P.C., 2001. A multi-block boundary element method for CFD/CSD grid interfacing. In: AIAA-2001-715, 39th Aerospace Science Meeting and Exhibit, Reno Nevada, USA.

Cho, M.H., Lee, I., 1994. Aeroelastic stability of hingeless rotors in hover using large deflection theory. AIAA Journal 32, 1472–1477.

Cho, M.H., Lee, I., 1995. Aeroelastic analysis of multibladed hingeless rotors in hover. AIAA Journal 23, 2348–2355.

De Andrade, D., Peters, D.A., 1993. Correlations of experimental flap–lag–torsion damping—a case study. In: Proceedings of the 49th Annual National Forum of the American Helicopter Society, St. Louis, MO, USA.

Dowell, E.H., Hall, K.C., Thomas, J.P., Florea, R., Epureanu, B.I. and Heeg, J., 1999a. Reduced order models in unsteady aerodynamics. In: AIAA/ASME/ASCE/AHS/ASC Structures, Structural Dynamics and Materials Conference, St. Louis, MO, USA.

Dowell, E.H., Hall, K.C., Thomas, J.P., Florea, R., Epureanu, B.I., Heeg, J., 1999b. Reduced order models in unsteady aerodynamics. AIAA Paper 99-1261.

Dowell, E.H., Hall, K.C., Thomas, J.P., Kielb, R.E., Spiker, M.A., Denegri Jr., C.M., 2006. Reduced order models in unsteady aerodynamics, aeroelasticity and molecular dynamics. In: Mota Soares, C.A., et al. (Eds.), II European Conference on Computational Mechanics Solids, Structures and Coupled Problems in Engineering, Lisbon, Portugal.

Eller, D., Carlsson, M., 2003. An efficient aerodynamic boundary element method for aeroelastic simulation and its experimental validation. Aerospace Science and Technology 7, 532–539.

Esfahanian, V., Behbahani-Nejad, M., 2002. Reduced order modeling of unsteady flows about complex configurations using the boundary element method. ASME Journal of Fluids Engineering 124, 988–993.

Feng, Z., Soulaimani, A., 2007. Reduced order modelling based on POD method for 3D nonlinear aeroelasticity. In: Proceedings of the 18th IASTED International Conference: Modelling and Simulation, Montreal, Canada, pp. 489–494.

Friedmann, P., Tong, P., 1972. Dynamic nonlinear elastic stability of helicopter rotor blades in hover and in forward flight. NASA CR-114485.

Greenberg, J.M., 1947. Airfoil in sinusoidal motion in a pulsating stream. NACA TN-1326.

Hall, K.C., 1994. Eigenanalysis of unsteady flows about airfoils, cascades, and wings. AIAA Journal 32, 2426–2432.

Hodges, D.H., Dowell, E.H., 1974. Nonlinear equations of motion for the elastic bending and torsion of twisted nonuniform rotor blades. NASA TN-7818.

Hodges, D.H., Ormiston, R.A., 1976. Stability of elastic bending and torsion of uniform cantilever rotor blades in hover with variable structural coupling. NASA TN D-8192.

IMSL Library reference manual, 1980. IMSL LIB-0008.

Katz, J., Maskew, B., 1988. Unsteady low-speed aerodynamic model for complete aircraft configurations. Journal of Aircraft 25, 302–310.

Katz, J., Plotkin, A., 2002. Low-Speed Aerodynamics, second ed. Cambridge University Press, New York.

Kim, T., 1998. Frequency-domain Karhunen–Loeve method and its application to linear dynamic systems. AIAA Journal 36, 2117–2123.

Kocurek, J.D., Tangler, J.L., 1977. A prescribed wake lifting surface hover performance analysis. Journal of the American Helicopter Society 22, 24–35.

Kwon, O.J., Hodges, D.J., Sankar, L., 1991. Stability of hingeless rotors in hover using three-dimensional unsteady aerodynamics. Journal of the American Helicopter Society 36, 21–31.

Landgrebe, A.J., 1972. The wake geometry of a hovering helicopter rotor and its influence on rotor performance. Journal of the American Helicopter Society 17, 3–15.

Loewy, R.G.A., 1957. Two dimensional approaches to the unsteady aerodynamics of rotary wings. Journal of the Aeronautical Sciences 24, 81–92.

Pomin, H., Wagner, S., 2002. Navier–Stokes analysis of helicopter rotor aerodynamics in hover and forward flight. Journal of Aircraft 39, 813–821.

Romanowski, M.C., 1996. Reduced order unsteady aerodynamic and aeroelastic models using Karhunen–Loeve eigenmodes. AIAA Paper 96-3981.

Shahverdi, H., 2006. Aeroelastic analysis of helicopter rotor blades using reduced order aerodynamic model. Ph.D. Dissertation, Amirkabir University of Technology, Tehran, Iran.

Shahverdi, H., Nobari, A.S., Behbahani-Nejad, M., Haddadpour, H., 2007. An efficient reduced-order modeling approach based on fluid eigenmodes and boundary element method. Journal of Fluids and Structures 23, 143–153.

Sharpe, D.L., 1986. An experimental investigation of the flap–lag–torsion aeroelastic stability of a small scale hingeless helicopterr in hover. NASA TP-2546.

Smith, M.J., 1996. Acceleration techniques for an aeroelastic Euler method for a hovering rotor. Journal of Aircraft 23, 429–434.

Tang, D., Dowell, E.H., Hall, K.C., 1999. Limit cycle oscillations of a cantilevered wing in low subsonic flow. AIAA Journal 37, 364–371.

Tang, D., Dowell, E.H., 2001. Effects of angle of attack on nonlinear flutter of a delta wing. AIAA Journal 39, 15–21.

Thomas, J.P., Hall, K.C., Dowell, E.H., 1999. Reduced order modelling of unsteady small-disturbance flows using a frequency-domain proper orthogonal decomposition technique. AIAA Paper 99-0655.

Yoo, K.M., Hodges, D.H, Peters, D.A., 1992. An interactive numerical procedure for rotor aeroelastic stability analysis using lifting surface. In: Proceedings of the 18th ICAS Conference, Beijing, PRC, pp. 1272–1280.